JACS
JOURNAL OF THE AMERICAN CHEMICAL SOCIETY

COMMUNICATION

pubs.acs.org/JACS

Directed Organization of C_{70} Kagome Lattice by Titanyl Phthalocyanine Monolayer Template

Yinying Wei† and Janice E. Reutt-Robey*

Department of Chemistry and Biochemistry, University of Maryland, College Park, Maryland 20742, United States

Supporting Information

ABSTRACT: Controlled deposition of titanyl phthalocyanine (TiOPc) on Ag(111) produces a honeycomb monolayer phase consisting of TiOPc molecules with two distinctive tilt angles. This periodic arrangement of polar molecules is used to direct C_{70} growth into low-density 3D films with novel C_{70} kagome lattice arrangements. Structural models for the C_{70} kagome lattice are determined from layer-by-layer scanning tunneling microscopy images and related to the dipolar TiOPc template and C_{70}'s anisotropic polarizability. Molecular templates with designed electrostatic features offer a practical method to control 3D film organization on the nanoscale by harnessing anisotropic molecular interactions at the growth interface.

A decade of intense study of fullerene films supported on metallic and semiconducting substrates has provided detailed structural information and property development.[1] While much work has focused on C_{60}-based films, C_{70} has also attracted interest for distinct morphological and electrostatic features that arise from its reduced symmetry.[2] Two prominent differences between C_{60} and C_{70} are shape and polarizability. The ellipsoidal C_{70} has curved π-conjugated surfaces, leading to concave−convex $\pi-\pi$ interactions distinct from those between two flat surfaces.[3] The electric dipole polarizability of C_{70} exceeds that of C_{60} by 25%,[2a] enhancing electrostatic interactions between C_{70} molecules as well as with other small organic molecules. Recently, C_{70}, incorporated as PCBM[C_{70}], has demonstrated a significant improvement in organic photovoltaic cell efficiency over PCBM[C_{60}]-based devices.[4] This follows theoretical predictions that C_{70} accepts more charge transfer from donating molecules, by comparison with C_{60}.[5]

The distinct molecular properties of C_{70} are expected to impact its organization in thin-film structures. In surface science, there are many examples of arranging the two-dimensional (2D) organization of molecular materials through templated assembly.[6] However, directing the three-dimensional (3D) spatial organization of films that contain small molecules and fullerenes still remains an important challenge.[7] Electrostatic interactions allow the rational design of 2D assemblies and structure prediction in molecular crystal engineering.[8] We now build upon this design concept by utilizing the polar titanyl phthalocyanine (TiOPc) molecule in a crystalline 2D phase to direct the C_{70} spatial organizations in 3D. The formation of a C_{70} kagome lattice is reported.

All molecular films were prepared *in situ* by physical vapor deposition and imaged at room temperature under ultrahigh-vacuum conditions. In a previous study, we described the formation and structure of a highly ordered TiOPc monolayer phase on Ag(111), designated as the honeycomb phase.[9] We summarize the structural features of this phase in Figure 1a−c; the monolayer contains three TiOPc molecules per unit cell (Figure 1b), including two tilted TiOPc molecules and one flat-lying TiOPc. Pairs of alternately tilted molecules comprise the honeycomb frame, while the flat-lying molecule occupies the honeycomb pore sites (Figure 1c). The TiOPc tilt angle was deduced from the symmetry, packing density, and 2.08 nm unit cell size by taking into account the finite 1.25 nm TiOPc molecular dimension. The tilt angle of ca. 40° prevents steric overlap and places the outermost phenyl rings and titanyl oxygen at comparable height. Striking scanning tunneling microscopy (STM) images are obtained because tilted TiOPc molecules appear as bright triangles and flat-lying TiOPc molecules appear dim.

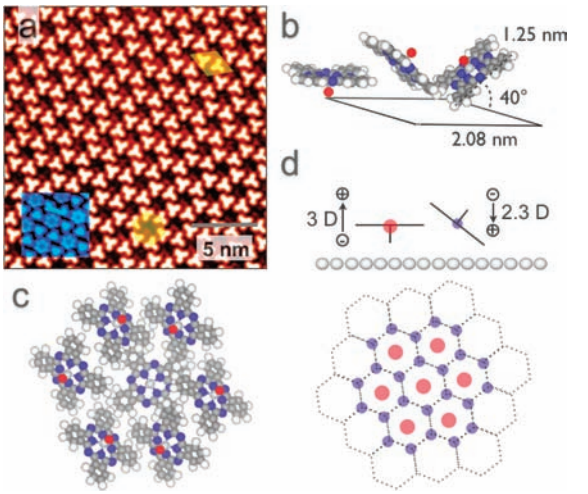

Figure 1. TiOPc honeycomb monolayer template. (a) Molecularly resolved STM image with honeycomb cell and unit cell shaded yellow (−0.7 V, 0.06 nA). Inset: imaged with reverse bias (0.8 V, 0.01 nA). (b) Side view of unit-cell molecules (yellow rhombus in panel a): two tilted TiOPc (honeycomb frame) and one flat-lying TiOPc (honeycomb pore). (c) Top-down view of honeycomb cell (yellow hexagon in panel a). (d) Schematic dipole lattice from monolayer of polar TiOPc. Side view illustrates vertical dipole moments for pore−TiOPc (red) and pairs of tilted TiOPc molecules (blue). Top-down view illustrates periodicity (size of colored spheres denotes relative dipole strength).

Received: April 1, 2011
Published: September 02, 2011

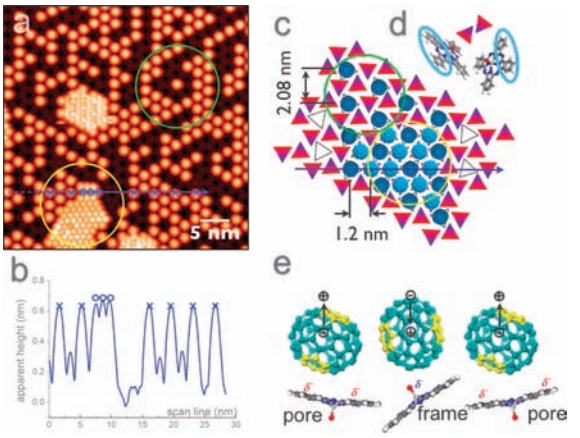

Figure 2. First-layer C_{70} on TiOPc template. (a) STM image shows C_{70} positioned directly above pore−TiOPc molecules (green circle) and close-packed C_{70} structures spanning the TiOPc network (yellow circle) (−0.87 V, 0.02 nA). (b) Line profile from panel a: blue line, isolated C_{70} above pore−TiOPc (marked as ×) and in close-packed island (marked as ○). C_{70} on pore−TiOPc has the lowest apparent height. (c) Model for first-layer adsorption shows C_{70} above pore−TiOPc and frame−TiOPc as dark and light blue, respectively. (d) Key for TiOPc representation as triangles in panel c. Blue depicts TiO apex; red depicts two adjacent phenyl rings. (e) Schematic side view of a static configuration depicting C_{70} anisotropy. Black arrows denote vertical component of C_{70} induced dipole.

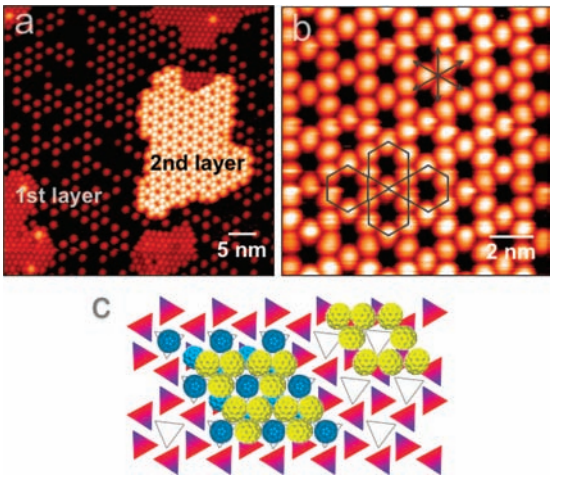

Figure 3. Second-layer C_{70} on TiOPc template. (a) STM image of second-layer C_{70} nucleated over the hcp first-layer C_{70} regions (0.87 V, 0.04 nA). (b) The "kagome" second-layer C_{70} structure. Gray lines emphasize the hexagons, trigons, and 120°-rotated C_{70} orientations. (c) Corresponding structural model of second-layer C_{70} (yellow), occupying bridge sites of two "C_{70}-on-frame" in the first-layer C_{70} (light blue), and its registration to TiOPc template (upper right corner).

Pore−TiOPc molecules are imaged with enhanced resolution at positive sample bias, as shown in the Figure 1a inset. Each pore−TiOPc exhibits six lobes in these room-temperature images. The 1.3 nm hexagon diameter is comparable to the hard-sphere TiOPc molecular width, indicating that the pore−TiOPc molecule adsorbs nearly parallel to the Ag surface and rotates at room temperature. The six lobes are attributed to the superposition of six energetically favorable adsorption configurations, reminiscent of CuPc adsorbed on a six-fold-symmetry C_{60} substrate.[6f] The structural model of Figure 1b directs the Ti−O group toward the surface based upon the topographic depression at the axial position, consistency with the bulk crystal structure of TiOPc, and growth patterns reported for TiOPc on HOPG.[10]

This TiOPc honeycomb monolayer is next utilized as a template for C_{70} growth. Films of C_{70}, grown layer-by-layer, yield 3D arrangements of unusually low density, demonstrating the long-range influence of the TiOPc template on C_{70} packing and orientation. An STM image of first-layer C_{70} grown on this TiOPc template is shown in Figure 2a. At the deposition onset, C_{70} occupies sites above pore−TiOPc molecules (green circle). The nearest-nighbor C_{70}−C_{70} distance of 2.08 nm directly corresponds to the pore−pore distance in the underlying TiOPc network. With increasing C_{70} coverage, small areas of hexagonal close-packed (hcp) C_{70} (1.2 nm nearest-neighbor distance) are observed (yellow circle). The C_{70} on pore−TiOPc sites appears slightly lower than C_{70} on frame−TiOPc, as shown in Figure 2b. The underlying TiOPc structure is unaltered by C_{70} deposition, and C_{70} registration with respect to the base TiOPc lattice is clearly determined. First-layer C_{70} structure is thermally stable at temperatures up to 450 K.

Based on these observations, a structural model for the first C_{70} layer is deduced, as shown in Figure 2c. The model illustrates how C_{70} molecules decorate pore−TiOPc sites (dark blue color) at lower coverage and nucleate into hcp islands with increased coverage. In these hcp islands, C_{70} molecules occupy both pore− and frame−TiOPc sites. The registration and lateral dimensions in the model match experimental STM observations. Highlighted C_{70} orientations in this schematic are discussed in the following paragraph. We subsequently use the expressions "C_{70}-on-frame" and "C_{70}-on-pore" to represent C_{70} on the different adsorption sites in the first layer.

The spherical appearance of all first-layer C_{70} molecules in room-temperature images suggests free rotation on the slow time scale of STM imaging. A heuristic model of the static layer structure can be obtained from the anisotropic properties of C_{70}. The concave π surfaces on C_{70} (yellow-shaded facets in Figure 2e) are known to interact most strongly with other small organic molecules,[3b,5] and local interactions between the concave π surfaces on C_{70} and the peripheral phenyl groups on TiOPc are stabilizing. Moreover, orientations with the long (most polarizable)[2b] C_{70} axis aligned to the TiOPc dipole axis will be favored electrostatically. A configuration that incorporates these two stabilizing influences of C_{70} anisotropy is shown schematically in Figure 2e. This static configuration provides a qualitative basis for understanding the formation of kagome lattice structures in multilayer films.

With increasing C_{70} deposition, second-layer C_{70} starts to grow above the first-layer close-packed C_{70} islands before the first C_{70} layer is complete, as is typical in organic beam epitaxy.[11] A large area of second-layer C_{70} is shown in Figure 3a. Unlike C_{70}'s typical growth habit, second-layer C_{70} on the TiOPc template is not close-packed.[12] Instead, second-layer C_{70} forms a "kagome" lattice, as shown in the magnified STM image in Figure 3b. In this kagome lattice, C_{70} molecules organize into hexagons and trigons. Centers of neighboring hexagons in the kagome structure are spaced at 2.08 nm and in registration with "C_{70}-on-pore". Furthermore, second-layer C_{70} molecules appear ellipsoidal in STM topographs, indicating a lying-down configuration. The three C_{70} molecules comprising the trigon have distinct 120°-rotated orientations, as indicated by arrows in Figure 3b.

dx.doi.org/10.1021/ja206175c |J. Am. Chem. Soc. 2011, 133, 15232–15235

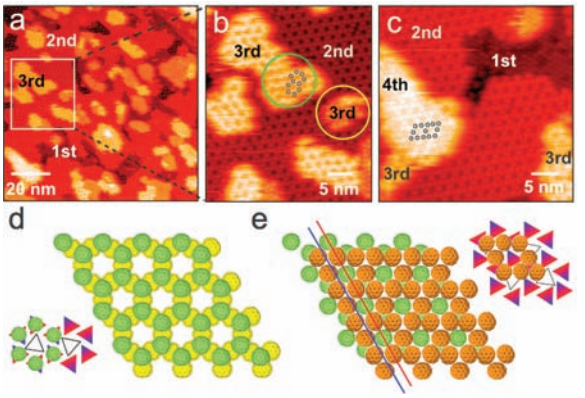

Figure 4. Successive C_{70} layers on TiOPc template. (a) STM view of multilayer structure (0.87 V, 0.04 nA). (b) Molecular details of third-layer C_{70}: C_{70} honeycomb (green circle) and C_{70} hexagonal island (yellow circle). (c) Kagome structure (marked in black) in fourth-layer C_{70}. (d) Structural model of third-layer C_{70} (light green) honeycomb and its registration to TiOPc template. (e) Structural model of fourth-layer C_{70} (orange) kagome structure and its registration to TiOPc template. Red and blue lines denote the offset between fourth (red line) and third (blue line) C_{70} layers.

A structural model for the second-layer C_{70} is depicted in Figure 3c, based directly on the STM images: The close packed first-layer structure consists of "C_{70}-on-frame" (light blue) and "C_{70}-on-pore" (dark blue). The second-layer C_{70} molecules (yellow) adopt bridge sites above two neighboring "C_{70}-on-frame" molecules in the first layer. As shown in the upper right corner of Figure 3c, this corresponds to the bridge sites of neighboring frame−TiOPc molecules in the TiOPc template. This arrangement maximizes the 3D coordination number of second-layer C_{70}. Moreover, the lying-down orientation of second-layer C_{70}, indicated by the elliptical shapes, offers favorable intermolecular interactions between the convex−concave π surfaces of first-layer and second-layer C_{70}. Second-layer C_{70} molecules thus form the "kagome" structure with four nearest-neighbor molecules in-plane, as observed in the STM images.

Multilayer film structures are very stable with respect to STM imaging under our measurement conditions (gap resistance $>2 \times 10^{10}$ Ω). Film structure evolution could thus be tracked through five layers with molecular resolution. Two distinct third-layer structures are observed in Figure 4, a honeycomb pattern (green circle in Figure 4b) and a close-packed structure (yellow circle in Figure 4b). The honeycomb pattern, emphasized with black dots in Figure 4b, is the dominant structure whose molecular packing model is suggested with light green C_{70} in Figure 4d. Third-layer "honeycomb" C_{70} molecules sit directly on the hollow position of the second layer and register vertically with the base frame−TiOPc molecules, as shown in the lower left corner of Figure 4d. The simultaneous growth of both the honeycomb and close-packed structures for third-layer C_{70} indicates that the influence of the TiOPc template on C_{70} growth begins to wane within the third layer.

The fourth layer repeats the second-layer C_{70} kagome structure, albeit with a lateral shift in registration. A molecular packing model is presented in Figure 4e. Fourth-layer C_{70} molecules register imperfectly with the base TiOPc template, as demonstrated in the upper right corner of Figure 4e. At the fifth layer, C_{70} molecules assume a bulk-like growth habit that continues in successive layers, as shown in the Supporting Information, Figure S2. Hexagonal close-packed domains in these ultrathin (5 nm) films are limited to 20−30 nm in the lateral dimension. Grain boundaries, dislocations, and even reconstructions are observed, reflecting the internal stress in these heterointerfaces.

We have tracked the layer-dependent formation of a C_{70} kagome lattice on a TiOPc monolayer template. To our knowledge, this is the first report of direct STM imaging of 3D kagome lattice structure formation in a small molecular system, while previous reports have been restricted to structures formed from colloidal crystals or magnetic molecular systems.[13] Such nanoporous structures, observed here for C_{70} films of 1−5 nm thickness, are distinct from structures reported for multilayer films of planar aromatic hydrocarbons. While films of perylene and PTDCA exhibit varying molecular orientations in the thin-film phases,[11,14] C_{70} exhibits unique low-density packing motifs.

We next relate these packing motifs to the electrostatic features of the TiOPc template. The honeycomb arrangement of polar TiOPc molecules may be viewed as a dipolar lattice. The strength of this dipolar lattice depends upon the free TiOPc molecular dipole, the monolayer structure, dipole−dipole interactions, and the extent of TiOPc−Ag(111) charge transfer. Based upon direct measurements of the surface dipole for the TiOPc/HOPG system,[15] and the generally weaker interface dipoles for nonpolar phthalocyanines on Ag(111),[16] we can roughly estimate the strength of this dipole lattice from a simple geometric analysis of free-molecular moments. For the tilted TiOPc molecules that constitute the honeycomb frame, the molecular dipole moment is partially canceled by the interlocked pairing, leaving a net vertical dipole of ca. +2.3 D per molecule, as per Figure 1d. Pore−TiOPc molecules, in contrast, retain the net dipole moment of ca. −3 D due to their flat-lying orientation. A schematic of this dipolar lattice is provided in Figure 1e, where dot size denotes the estimated strength and color denotes direction.

Kagome lattice formation in the highly polarizable C_{70} appears to be induced by this dipolar lattice: First-layer C_{70} adopts a close-packed arrangement and TiOPc registration that is stabilized by both $\pi-\pi$ and dipole−induced dipole interactions between C_{70}−TiOPc and C_{70}−C_{70}, as depicted in Figure 2e. Second-layer C_{70} seeks bridge sites between neighboring "C_{70}-on-frame" (equivalent to the bridge sites of frame−TiOPc) in the first layer, maximizing 3D coordination and electrostatic interaction with the first-layer C_{70}. This optimization evidently leads to the formation of the low-density kagome structure. Third-layer C_{70} molecules occupy the hollow sites of the trigons in the second-layer kagome structures, retaining registration with the base TiOPc template. The fourth-layer C_{70} repeats the "kagome" structure of the second layer, but with a lateral shift that breaks registration to the base TiOPc template. Under the room-temperature growth conditions, the bulk-like C_{70} close-packing structure commences with fifth-layer C_{70}, at a height of 5 nm above the dipolar TiOPc template.

We have performed further chemical tests to assess the importance of C_{70} anisotropy and TiOPc layer structure on kagome lattice formation: (1) Substituting C_{60} for C_{70}, we explored structural evolution of spherical fullerenes on the TiOPc honeycomb template. At very low coverage, isolated C_{60} molecules occupy pore−TiOPc sites, as per the C_{70} case; however, even at submonolayer C_{60} amounts, C_{60} and TiOPc spontaneously phase-separate into hexagonal C_{60} domains and TiOPc honeycomb domains (Supporting Information, Figure S3). The absence of a close-packed first-layer C_{60} structure on TiOPc,

such as that observed for C_{70} (Figure 2a), is consistent with our interpretation of C_{70} first-layer structure: C_{60} lacks the anisotropic shape and polarizability needed to stabilize the C_{60} first-layer structure. (2) In a second test, C_{70} was deposited on a different TiOPc monolayer phase (the hexagonal phase), which has a uniform TiOPc orientation that should give rise to weaker electrostatic interactions with C_{70} (Supporting Information, Figure S4). C_{70} deposition on a hexagonal TiOPc monolayer similarly reveals an unstable interface that spontaneously rearranges into C_{70} and TiOPc monolayer domains and cocrystalline domains that directly contact the Ag(111) substrate.

In conclusion, we have used monolayer films of the polar TiOPc molecule for templated C_{70} 3D spatial organization. Multilayer films with distinctive low-density C_{70} packing were measured, and layer-by-layer structure models were developed. The formation of a molecular-level kagome lattice was interpreted through geometric (packing) and qualitative analysis of electrostatic interactions. Measured structure features (registration, coordination number) were related to the base dipolar lattice. As C_{60} does not produce similar porous structures on the TiOPc honeycomb lattice, despite its similar "footprint", C_{70} appears particularly amenable to such directed organization. This is attributed to the ellipsoidal shape, curved surfaces, and higher dipole polarizability of C_{70}, leading to stronger and more anisotropic intermolecular interactions. These properties render C_{70} promising for applications in photovoltaic cells, in which vertical segregation of component materials is desired,[4a] and molecular sensors, in which 3D porous structures are highly sought.[17]

■ ASSOCIATED CONTENT

Supporting Information. Charge distribution for an individual TiOPc molecule determined by DFT calculation; STM images of multilayer C_{70} structures grown on top of TiOPc template, C_{60} molecules grown on top of TiOPc honeycomb template, and C_{70} grown on hexagonal TiOPc phase. This material is available free of charge via the Internet at http://pubs.acs.org.

■ AUTHOR INFORMATION

Corresponding Author
rrobey@umd.edu

Present Addresses
[†]Interdisciplinary Nanoscience Center and Department of Physics and Astronomy, Aarhus University, DK 8000 Aarhus C, Denmark

■ ACKNOWLEDGMENT

This work has been supported by the National Science Foundation under Surface Analytical Chemistry grant CHE-0750203 and by the University of Maryland under grant MRSEC DMR-05-20471.

■ REFERENCES

(1) (a) Altman, E. I.; Colton, R. J. *Phys. Rev. B* **1993**, *48*, 18244. (b) Guo, S.; Nagel, P. M.; Deering, A. L.; Van Lue, S. M.; Kandel, S. A. *Surf. Sci.* **2007**, *601*, 994. (c) Katsonis, N.; Marchenko, A.; Fichou, D. *Adv. Mater.* **2004**, *16*, 309. (d) Moriarty, P. J. *Surf. Sci. Rep.* **2010**, *65*, 175. (e) Sakurai, T.; Wang, X. D.; Xue, Q. K.; Hasegawa, Y.; Hashizume, T.; Shinohara, H. *Prog. Surf. Sci.* **1996**, *51*, 263.

(2) (a) Compagnon, I.; Antoine, R.; Broyer, M.; Dugourd, P.; Lerme, J.; Rayane, D. *Phys. Rev. A* **2001**, *64*, 025201. (b) Zope, R. R. *J. Phys. B-At. Mol. Opt.* **2007**, *40*, 3491. (c) Saito, S.; Oshiyama, A. *Phys. Rev. B* **1991**, *44*, 11532. (d) Silly, F.; Shaw, A. Q.; Porfyrakis, K.; Briggs, G. A. D.; Castell, M. R. *Appl. Phys. Lett.* **2007**, *91*, 253109.

(3) (a) Kawase, T.; Kurata, H. *Chem. Rev.* **2006**, *106*, 5250. (b) Vilmercati, P.; Castellarin-Cudia, C.; Gebauer, R.; Ghosh, P.; Lizzit, S.; Petaccia, L.; Cepek, C.; Larciprete, R.; Verdini, A.; Floreano, L.; Morgante, A.; Goldoni, A. *J. Am. Chem. Soc.* **2009**, *131*, 644.

(4) (a) Pfuetzner, S.; Meiss, J.; Petrich, A.; Riede, M.; Leo, K. *Appl. Phys. Lett.* **2009**, *94*, 223307. (b) Sakai, J.; Taima, T.; Yamanari, T.; Saito, K. *Sol. Energy Mater. Sol. Cells* **2009**, *93*, 1149.

(5) Wang, Y. B.; Lin, Z. Y. *J. Am. Chem. Soc.* **2003**, *125*, 6072.

(6) (a) Blunt, M. O.; Russell, J. C.; Gimenez-Lopez, M. D.; Taleb, N.; Lin, X. L.; Schroder, M.; Champness, N. R.; Beton, P. H. *Nat. Chem.* **2011**, *3*, 74. (b) Bonifazi, D.; Kiebele, A.; Stohr, M.; Cheng, F. Y.; Jung, T.; Diederich, F.; Spillmann, H. *Adv. Funct. Mater.* **2007**, *17*, 1051. (c) Dante, M.; Yang, C.; Walker, B.; Wudl, F.; Nguyen, T. Q. *Adv. Mater.* **2010**, *22*, 1835. (d) Xu, B.; Zhu, E. K.; Lu, C.; Liu, Y. D.; Liu, Z. Y.; Yu, D. L.; He, J. L.; Tian, Y. J. *Appl. Phys. Lett.* **2010**, *96*, 072109. (e) Chen, T.; Pan, G. B.; Yan, H. J.; Wan, L. J.; Matsuo, Y.; Nakamura, E. *J. Phys. Chem. C* **2010**, *114*, 3170. (f) Fendrich, M.; Wagner, T.; Stohr, M.; Moller, R. *Phys. Rev. B* **2006**, *73*, 115433.(g) Yoshimoto, S.; Kobayashi, N. In *Functional Phthalocyanine Molecular Materials*; Jiang , J., Ed.; Springer: Berlin, 2010; Vol. 135, p 137. (h) Bartels, L. *Nat. Chem.* **2010**, *2*, 87.

(7) De Feyter, S. *Nat. Chem.* **2011**, *3*, 14.

(8) (a) Day, G. M.; Motherwell, W. D. S.; Jones, W. *Cryst. Growth Des.* **2005**, *5*, 1023. (b) Stepanow, S.; Ohmann, R.; Leroy, F.; Lin, N.; Strunskus, T.; Woll, C.; Kern, K. *ACS Nano* **2010**, *4*, 1813.

(9) Wei, Y. Y.; Robey, S. W.; Reutt-Robey, J. E. *J. Phys. Chem. C* **2008**, *112*, 18537.

(10) Kera, S.; Abduaini, A.; Aoki, M.; Okudaira, K. K.; Ueno, N.; Harada, Y.; Shirota, Y.; Tsuzuki, T. *Thin Solid Films* **1998**, *327*, 278.

(11) Hanel, K.; Sohnchen, S.; Lukas, S.; Beernink, G.; Birkner, A.; Strunskus, T.; Witte, G.; Woll, C. *J. Mater. Res.* **2004**, *19*, 2049.

(12) (a) Gimzewski, J. K.; Modesti, S.; David, T.; Schlittler, R. R. *J. Vac. Sci. Technol. B* **1994**, *12*, 1942. (b) Wang, X. D.; Yurov, V. Y.; Hashizume, T.; Shinohara, H.; Sakurai, T. *Phys. Rev. B* **1994**, *49*, 14746.

(13) (a) Chen, Q.; Bae, S. C.; Granick, S. *Nature* **2011**, *469*, 381. (b) Maspoch, D.; Ruiz-Molina, D.; Veciana, J. *J. Mater. Chem.* **2004**, *14*, 2713.

(14) (a) Chen, Q.; Rada, T.; McDowall, A.; Richardson, N. V. *Chem. Mater.* **2002**, *14*, 743. (b) Chen, Q.; McDowall, A. J.; Richardson, N. V. *Langmuir* **2003**, *19*, 10164. (c) Chen, Q.; McDowall, A. J.; Richardson, N. V. *Chem. Mater.* **2003**, *15*, 4113. (d) Beernink, G.; Strunskus, T.; Witte, G.; Woll, C. *Appl. Phys. Lett.* **2004**, *85*, 398. (e) Witte, G.; Woll, C. *J. Mater. Res.* **2004**, *19*, 1889. (f) Marchetto, H.; Groh, U.; Schmidt, T.; Fink, R.; Freund, H. J.; Umbach, E. *Chem. Phys.* **2006**, *325*, 178.

(15) (a) Kera, S.; Yabuuchi, Y.; Yamane, H.; Setoyama, H.; Okudaira, K. K.; Kahn, A.; Ueno, N. *Phys. Rev. B* **2004**, *70*, 085304. (b) Fukagawa, H.; Yamane, H.; Kera, S.; Okudaira, K. K.; Ueno, N. *Phys. Rev. B* **2006**, *73*, 041302. (c) Fukagawa, H.; Hosoumi, S.; Yamane, H.; Kera, S.; Ueno, N. *Phys. Rev. B* **2011**, *83*, 085304.

(16) Molodtsova, O. V.; Grobosch, M.; Knupfer, M.; Aristov, V. Y. *Appl. Phys. Lett.* **2007**, *91*, 244103.

(17) Mintova, S.; Bein, T. *Microporous Mesoporous Mater.* **2001**, *50*, 159.